

FREESE, *NEAL, and LENOE

LEVEL II

①

AD A056436

11 JUN 1978

DDC
RECEIVED
JUL 10 1978

6 PROOF TEST PROCEDURES FOR CERAMIC MISSILE RADOMES

10 COLIN E. FREESE, MR., *DONALD M. NEAL, MR., and EDWARD M. LENOE PhD
ARMY MATERIALS AND MECHANICS RESEARCH CENTER
WATERTOWN, MASSACHUSETTS 02172

12/15p/

INTRODUCTION

Currently ceramics are used for radome structures in several Army missiles because of their desirable dielectric properties, in addition to rain erosion resistance. The use of brittle ceramic materials as in radome structural components is relatively new. Since each radome developed requires a new design, it is important to thoroughly understand the materials capabilities. Ceramics rarely exhibit a single characteristic failure strength and therefore uncertainty exists regarding stress levels to which they can be safely subjected. The common concept of ceramic fracture is that of failure initiation due to tensile stresses acting at the size of a stress-intensifying flaw. Such flaws are either basic features of the microstructure, namely pores, inclusions, weak grain boundaries, or external scratches or cracks introduced during surface finishing or handling. In many structural ceramics variability of worst flaws leads to a size dependency of strength (1,2). Therefore recognition of variability in strength is important for proper structural design of these materials. This variability usually requires a probability-based failure criteria such as the Weibull representation. That is

$$P_f = 1 - \exp \left[-K \int_V (\sigma - \sigma_u / \sigma_0)^m dV \right] \quad (1)$$

where K is related to loading, V is the volume of material, σ is fracture stress, and σ_u is threshold stress; σ_u is defined as zero for the particular brittle materials considered in this paper; σ_0 and m are distribution constants determined from test data.

78 06 12 029

DISTRIBUTION STATEMENT A

Approved for public release;
Distribution Unlimited

403 105

JOB

ADJ NO.
DDC FILE COPY

FREESE, *NEAL, and LENOE

Consideration of time-dependent failure is also important. Fracture is delayed, occurring after stress has been sustained for some duration. Associated with the phenomena of static fatigue is an increase in strength with increase in stress or strain rates (3,4). For silicate glasses and most oxide ceramics it is known that the presence of moisture causes the environment to be reactive, even at ambient conditions (5). Numerous researchers have demonstrated the occurrence of subcritical crack growth in water and observed equivalent strength reductions in glass ceramics by a factor of one third and of alumina ceramic by one fourth. Thus the selection of a ceramic component should not be based on strength alone. The occurrence and rate of crack growth can be a decisive factor.

From the analytical viewpoint, theories are available and partially verified for treating the effects of time, size, and stress distribution on the likelihood of failure (6). From a pragmatic viewpoint, pre-service proof testing can also be applied. Effective proof testing must closely simulate not only the magnitude, but also the distribution of tensile stresses. In addition, proper account must be taken of any subcritical crack growth which might occur during attempted proof stressing.

DISCUSSION OF MATERIAL CHARACTERIZATION AND PROOF TEST PROCEDURES

In component qualification, it is important to consider a typical ceramic radome product specification (7). Requirements for mechanical properties data include hoop tensile strength as determined via hydrostatic internal pressurization of a thin ring. The specification calls for two strength determinations on rings machined from the base of each radome. Density determinations are made on failed segments subsequent to burst testing. Figure 1 illustrates a typical ring specimen and includes a schematic of test apparatus. Hoop tensile strength is calculated from an elementary strength-of-materials formula. The modulus of rupture or flexure test is also a qualification requirement. Samples are fabricated in the same manner as the radome and from the same casting slip. Three specimens are required. It is of interest that both types of tests are performed at room temperature. Some mechanical properties data were available in the open literature for slip-cast fused silicate (SCFS). Tensile evaluations were performed in a gas bearing tension facility. Strength observations were completed over temperatures ranging from 70 F to 2200 F. Figure 2 summarizes tensile strength versus failure probability for the coupon specimens. Also shown in this illustration are results from hydroburst ring tests for one particular type of SCFS radome (Type I). Note the significant difference in tensile strength for the coupon versus ring tests, and the

White Section	<input checked="" type="checkbox"/>	<input type="checkbox"/>
Dark Section	<input type="checkbox"/>	<input type="checkbox"/>
Per Basic rpt.		
ASC, vol. 1		
REPRODUCTION/AVAILABILITY NOTES		
DATE: 11/11/61 BY: J. E. B. / J. E. B.		
A		

78 06 12 029

FREESE, *NEAL, and LENOE

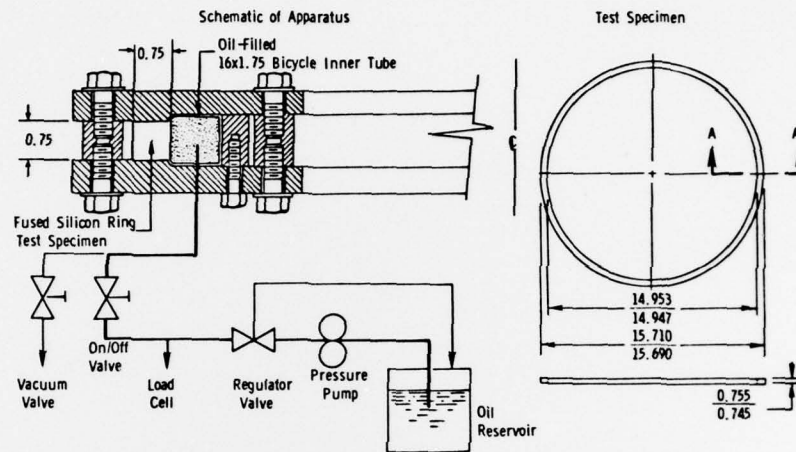


Figure 1. Hydroburst apparatus and test specimen

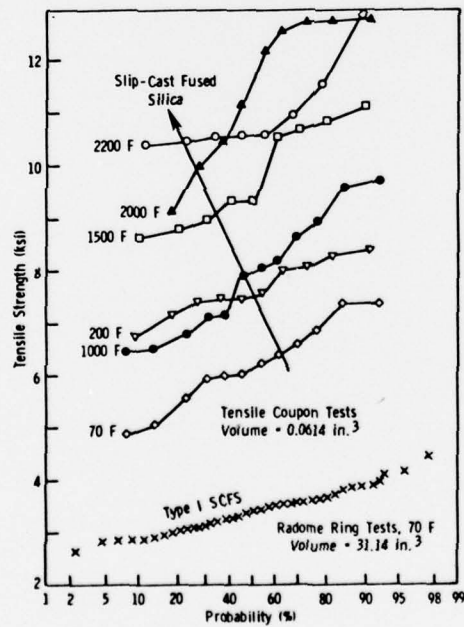


Figure 2. Temperature effects on tensile strength

difference in volume of the tension specimens. Interpretation of such phenomena has received a fair amount of attention (8,9). Based on the assumption that volume and/or surface area versus strength effects exist and furthermore can be well represented by Weibull statistics, numerous investigators have presented theoretical interrelationships to estimate the strength of a particular specimen geometry and load distribution from data obtained in different configurations. Suppose, for instance, we consider the case of uniform tension and assume strength is merely volume-dependent. Then at the same value of failure probability, for two distinct sets of statistical data,

$$\sigma_1/\sigma_2 = [(K_2V_2)/(K_1V_1)]^{1/m} \quad (2)$$

where σ_1, σ_2 are corresponding stresses, V_1, V_2 their associated volumes, and K_1, K_2 define the type of loading. Furthermore, a two-parameter Weibull representation has been assumed such that the probability of fracture at a given stress σ is taken as Eq. 1 with $\sigma_u = 0$ and the risk of rupture is defined as

$$R = \int_V (\sigma/\sigma_0)^m dV \quad (3)$$

Equation 3 can be evaluated for any given stress distribution appropriate to the experiment being conducted. Thus, simple interrelations can be developed for the variety of test methods applied to ceramics. Figure 3 summarizes data available for SCFS radomes. Data from each experimental apparatus is fit by the Weibull statistic and then the strength distribution of the other test method is estimated

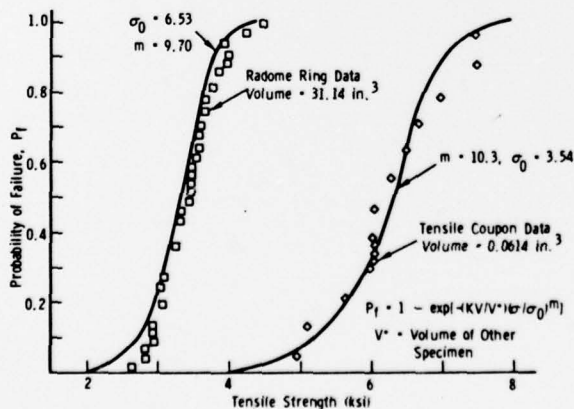


Figure 3. Size effects on tensile strength of slip-cast fused silica

and compared to observed response. Referring to Figure 3, it appears that the two-parameter Weibull model is a fairly good representation for the size/strength effect. As a further confirmation, experiments were conducted on Type I SCFS for three- and four-point flexure. Figure 4 summarizes these estimates and limited experimental data.

AEROTHERMAL TESTS

Typically aerothermal preflight certification tests are conducted on radome materials. Such tests are intended to simulate, to the extent possible, ascent and re-entry worst-case heating environments to screen candidate materials. Flight test risks on actual hardware rather than subscale models is used since numerous difficulties are inherent in aerothermal models. It is difficult, for instance, to accurately correlate subscale heat shield thicknesses, gaps, steps, protrusions, and boundary layer characteristics, with full-scale radome structures.

In operation, various gas combustors are used to impinge a high temperature exhaust with reasonable simulation of pressure and velocity characteristics. As an example, the ascent heating of the radome forebody is simulated by a relatively low preheat gas combustor and the radome removed and then allowed to equilibrate until a desired joint bond line temperature is achieved. Subsequently the radome is plunged into combustor exhaust. However, the gas is now at the appropriate temperatures to represent the re-entry phase of the simulation. Aerothermal tests are not considered in any detail in this report. Room temperature internal pressure tests such as illustrated in Figure 5 are considered in depth.

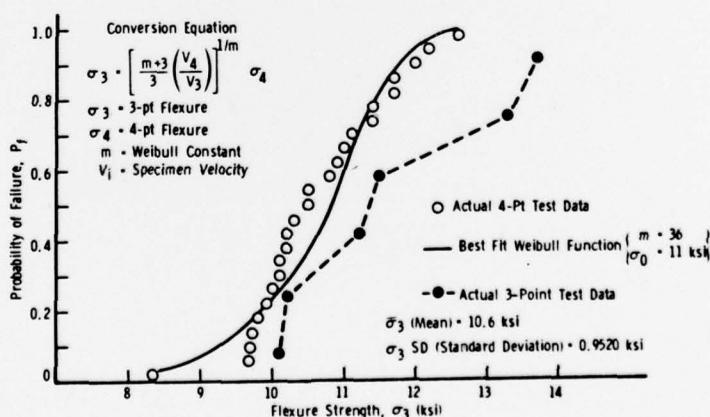


Figure 4. Estimates of three-point flexure strength from four-point flexure data

STATIC STRUCTURAL TESTS

Several types of static structural loadings are typically employed to verify load capacity, to assess structural integrity, or to proof test from the mechanical strength viewpoint. One experiment is depicted by Figure 5 wherein a radome is subjected to internal hydrostatic pressure. Figures 6 and 7 show experiments intended to verify load capacity of the radome and joint designs. In these instances the static tests employ whiffletree arrangements or simple off-angle loaded fabric straps. The load magnitudes are intended to simulate critical mission maneuver load magnitudes. The loads are applied quasi-statically and usually do not represent real mission times. The spatial distribution of loads is represented only in an approximate sense.

TIME DEPENDENCY

Time-dependent failure, or the possible existence of slow crack growth phenomena, had apparently not been investigated for SCFS typically used in missile radomes, therefore this aspect of material response was explored. Baseline data was obtained for Type I SCFS specimens prepared from radome fragments as well as specially prepared representative billets. Mechanical strength tests were performed at different loading rates. Differences in strength as a function of these stressing rates can be used to infer analytical models for slow crack growth. Based on such results, the so-called strength-probability-time (SPT) nomograph can be prepared (4). Such information is useful, for instance, in establishing proof test load limits and safety margins for long-term stress such as might be maintained by mismatch bonded or mechanical radome-to-substructure joints.

These beam specimens were subjected to ultrasonic and X-ray inspection and ultrasonic velocities were obtained as well as bulk densities. In this series of tests acoustic emission (AE) apparatus was additionally employed. The intention of the AE observations was to explore the possibility of detecting material damage prior to failure. These series of experiments did not yield any useful correlation between AE counts; neither total counts nor rate of emission gave a clear-cut trend with strength levels.

There were several objectives of the experiments on this SCFS. It was desired to thoroughly investigate slow crack growth at room temperature. Accordingly, flexure tests were conducted at each of two loading rates. This permitted construction of the SPT nomograph. In order to study the validity of this technique, a series of creep rupture tests were completed. These were compared to predicted failure times to substantiate the methodology, as discussed subsequently.

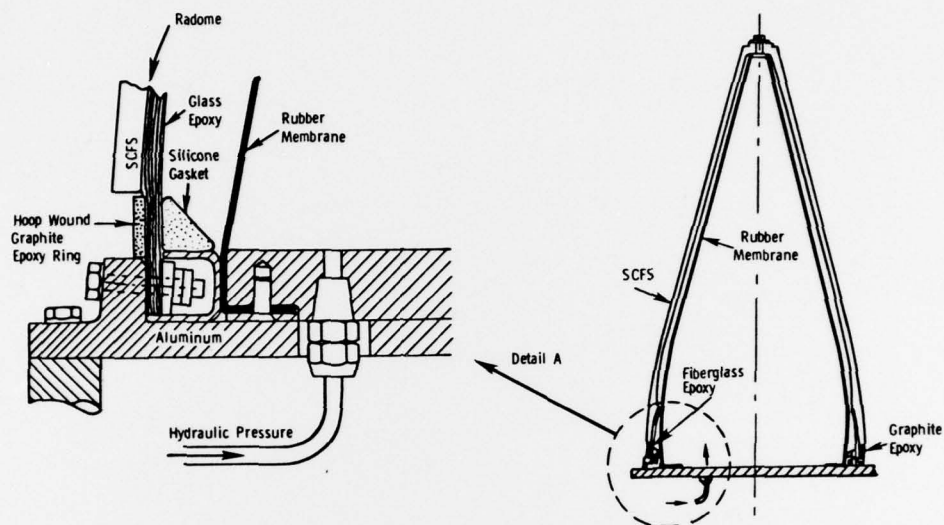


Figure 5. Internal pressurization radome proof test apparatus

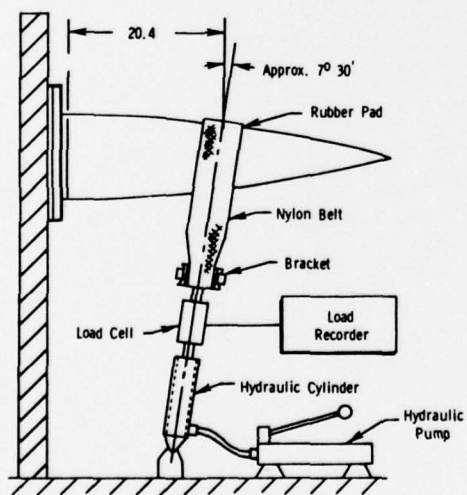


Figure 6. Schematic of off-axis joint proof test

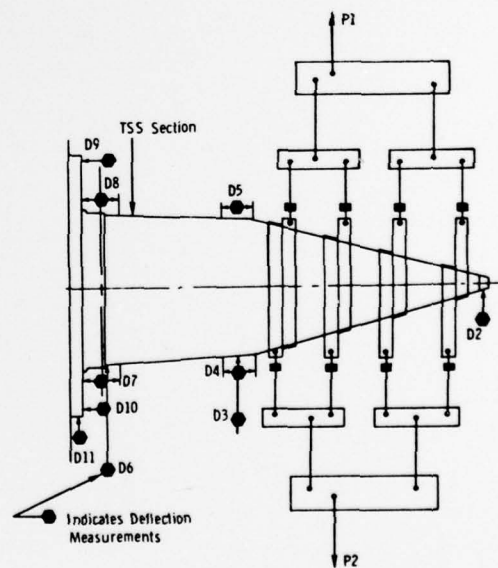


Figure 7. Schematic of whiffle-tree static test

FREESE, *NEAL, and LENOE

Another objective for this series of experiments was to study possible proof stress damaging effects on strength and/or time to failure of SCFS at ambient conditions. Therefore a set of virgin, e.g., untested, beams was loaded to predetermined stress levels and tested to failure (see Figure 8).

CONSTRUCTION OF THE DESIGN STRENGTH-PROBABILITY-TIME NOMOGRAPH

Under constant stress σ in a delayed fracture test, the time to failure T is given, in an elementary fashion, by:

$$T = \int_{C_i}^{C_{Ic}} dc/V \quad (4)$$

where C_i is initial crack size, C_{Ic} critical crack size, and V crack velocity. Assuming that a simple power form of crack velocity versus stress intensity can be written $V = \alpha K_{Ic}^n$, then

$$T = 2K_{Ic}^{2-n} / [(\sigma y)^2 \alpha (n-2)] \quad (5)$$

and for typical large n values, K_{Ic} are negligible. For a given batch of N specimens with initial flaw size C_j

$$T = \frac{2y^{2-n} \sigma^{2-n} C_j^{(2-n)/2}}{(\sigma y)^2 \alpha (n-2)} = \frac{BC_j^{(2-n)/2}}{\sigma^n}$$

where y = geometric constant. Then, for specimens with the same initial flaw size and the same probability of failure,

$$T\sigma^n = \alpha_1. \quad (6)$$

Using Eq. 6, a family of lines can be constructed on the Weibull strength/probability of survival graph corresponding to increasing failure times. For an individual specimen stressed at σ_1 and failing

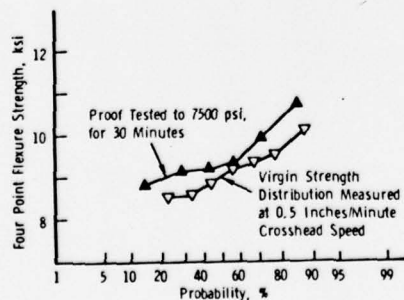


Figure 8. Effect of proof stress on flexure strength distribution

in T_1 , we now have a relationship for another specimen failing at stress σ_0 in a reference time T_0 . This permits construction of an SPT nomograph where a family of parallel lines are equispaced for equal logarithmic increases in failure time (4). According to this simple theory, creep rupture data can be related to instantaneous dynamic failure by use of the following relationship,

$$(\sigma_0/\sigma_j)^n = T_j/T_0 \quad (7)$$

DISCUSSION OF RATE EFFECTS

The SCFS specimens were machined to 0.11×0.15×2.0-inch sizes and tested in four-point bending (1.875-inch span) at room temperature, for a load rate of 0.5 in./min. Another group of 22 specimens was tested in the same manner except load rate was 0.01 in./min. The strength levels for each set of data were obtained. Results are plotted in Figure 9, indicating good fit to the Weibull distribution. It was determined from the test data at the 99% confidence level (10) that mean strength ($\bar{\sigma} = 9.07$ ksi) for load rate of 0.5 in./min was significantly greater than $\bar{\sigma} = 8.14$ ksi for the 0.01 in./min rate. An SPT diagram, Figure 10, was constructed using the data described above in conjunction with the theory discussed next. Failure times of 1.27 sec and 57.0 sec were determined for strength values of 9.07 and 8.14, respectively.

The exponent $n = 35.12$ from Eq. 7 is obtained from the strength and time data, providing the necessary parameters for SPT diagram construction. The Weibull modulus $m = 15.06$, describing the slope of time-to-failure lines in the SPT diagram, was determined from averaging m values obtained from the two different load rates.

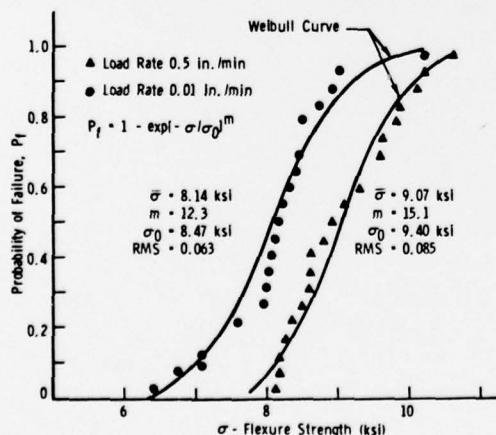


Figure 9. Load rate effects (SCFS)

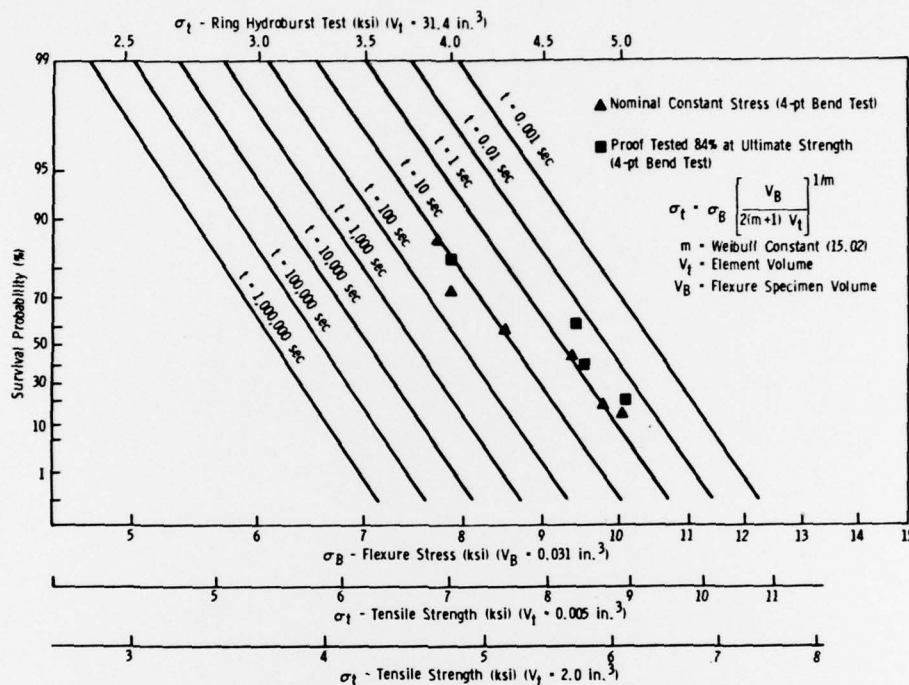


Figure 10. SPT diagram for SCFS superimposed delayed fracture data normalized to failure time of one second

An evaluation of the adequacy of the SPT diagrams for SCFS was made from delayed fracture data to estimate the equivalent failure stresses for a failure time of 1 second. Results in Figure 10 show excellent agreement between delayed fracture data and the predicted data, except for specimens failing within a short time frame ($T < 1$ minute). Figure 10 survival probabilities are represented as a function of both bend and tensile stress volumes (V_t). It should be noted that smaller V_t result in higher failure loads for equivalent P_s values. The flexure stress labelled with $V_B = 0.031 \text{ in.}^3$ represents the test results presented in this report. The equivalent data for a tension test were superimposed on the diagram to indicate the effects of volume changes. The σ_t values for $V_t = 0.005 \text{ in.}^3$ and 2.0 in.^3 are tabulated to provide ranges of probability versus stress for relatively small and large elements such as used in a finite element analysis. The label at the top of diagram where $V_t = 31.4 \text{ in.}^3$ represents the volume of the ring used in a hydroburst strength test to measure the quality of SCFS.

ANALYSIS OF THE INTERNAL PRESSURIZATION PROOF TEST

Thus far we have gained insight into the probability of failure and time dependency aspects of strength behavior. This information can now be used to assess the radome internal pressurization proof test depicted in Figure 5. For this purpose, an axisymmetric finite element analysis was performed using a unique set of finite element software modules. This approach has been shown to be both efficient and competitive (11) with other finite element procedures. The final result is a series of codes which address directly the particular structure in question and the types of information required. A primary concern with the effects of various end-restraint conditions isoparametric axisymmetric solid element was used to model the elastic behavior of the radome and a substructuring technique was implemented. The entire structure contains over 3000 degrees of freedom and is divided into four subregions, the details of which are shown in Figure 11.

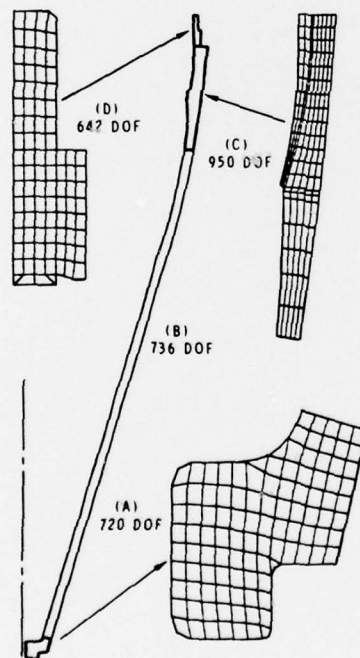


Figure 11. Finite element gridding

Several conditions were analyzed. First, the radome was assumed to be pressurized to 100 psi internal pressure (see Figure 5). This pressure was taken to act over the entire inner surface down to the aluminum restraining ring (see detail joint schematic, Figure 5). In the region of the retaining ring no radial movements were permitted on the outer surface of the radome. Two additional computations were completed wherein 7-mil and 15-mil radial displacements were imposed. These displacements are intended to simulate the effects of out-of-tolerance conditions which might occur and should be primarily applied to the inner surface of the restraint region due to the inability of the bolt-up configuration to transmit tensile loads. The entire structure can be treated for a unique set of boundary conditions in approximately six minutes (UNIVAC 1106) of computer time. A consideration of various restraint conditions applied to subregion (d) in Figure 11 can be achieved at a fraction of that cost.

Since axisymmetric conditions apply, the calculations of radial displacement effects are lower bound estimates. In reality, out-of-tolerance dimensions may be nonsymmetric.

Furthermore, in bolting the radome in place, the displacements would most likely be imposed sequentially on opposite ends of the diameter of the base. These facts, coupled with stress concentrations around bolt holes, suggest that somewhat larger stresses might exist due to mismatched tolerances.

ASSESSMENT OF PROBABILITY OF SURVIVAL

Results of the finite element stress analysis were used to estimate probability of survival under conditions of the proof test. Note that the radome joint consists of four types of material, namely SCFS, glass epoxy, graphite epoxy, and the joint adhesive. Accordingly, two analytical formulations were used. The finite element stress distributions were used in evaluating individual probability values of the finite volume elements of the SCFS structure and multiplying these probabilities to obtain P_s for the particular applied loads. The probability of survival P_s for individual stress components is written as

$$P_{s_i} = \exp [-KV_i/V^* (\sigma_{\max_i}/\sigma_0)^m] \quad (8)$$

where $K = 1$ for simple tensile stress, V_i = volume of elements, V^* = volume of test specimen, and σ_{\max_i} = maximum principal stress in element. The probability of survival P_s of the entire structure is

FREESE, *NEAL, and LENOE

$$P_s = \prod_{i=1}^N P_{s_i} \quad (9)$$

where N = number of elements in finite element solution.

Weibull strength parameters were $m = 10.30$ and $\sigma_0 = 3.55$ ksi, obtained from hydroburst tests on SCFS rings with 31.4 in.³ volume. Since fiberglass, graphite, and the adhesive materials are not assumed volume-dependent, reliability calculations for these materials were based on application of the Warner (stress-strength) diagram for each individual material element (12).

The reliability of these materials was determined from the basic concept that a no-failure probability exists when allowable stress S is not exceeded by applied stress s . That is,

$$R = \int_{-\infty}^{\infty} f(s) \left[\int_s^{\infty} f(S) dS \right] ds \quad (10)$$

where $f(s)$ is the probability density function obtained from knowledge of the design stress in the structural element and $f(S)$ represents the distribution of the material strength. The standard deviations for $f(s)$ and $f(S)$ are obtained from strength data and an assumed variability in design stress calculations. If density functions for strength and stress are assumed normal (12), then

$$R = [1/(\sigma_{\zeta}\sqrt{2\pi})] \int_0^{\infty} \exp \left[-1/2 \left((\zeta - \bar{\zeta})/\sigma_{\zeta} \right)^2 \right] d\zeta \quad (11)$$

where $\bar{\zeta} = \bar{S} - \bar{s}$, $\sigma_{\zeta} = \sqrt{\sigma_S^2 + \sigma_s^2}$, and $\zeta = S - s$. The σ_S and σ_s are standard deviations for strength and stress data.

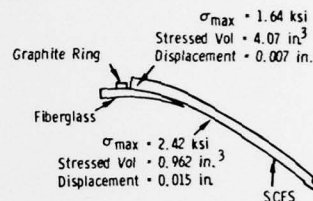
P_s calculations were completed for each material component and used in Eq. 9 to determine reliability of the entire structure, which includes the four materials. Important results of the calculations are summarized in Table 1, where the location and material with corresponding maximum stress and associated stressed volume are indicated. Sensitivity of the P_s estimates was also evaluated by assuming coefficients of variation of 0%, 10%, and 15% in stresses.

Table 1. RELIABILITY CALCULATIONS FROM
PROOF TEST OF RADOME

Displacements	CV (%) Design Stress	P_s Complete Radome	Material Peak P_f
0.000	0.000	0.99860	SCFS
.007	0.000	.99859	SCFS
.007	10.000	.99840	SCFS
.007	15.000	.99831	SCFS
.015	0.000	.96095	Graphite
.015	10.000	.89665	Graphite
.015	15.000	.79084	Graphite

 P_s = Probability of Survival P_s = 0.99989
(MM Rohm & Haas) P_f = Probability of Failure

STRENGTH MATERIALS (%)		
Materials	Mean Strength (ksi)	Standard Deviation (ksi)
SCFS	3.380	0.396
Adhesive	0.660	0.140
Graphite	80.000	8.000
Fiberglass	26.500	4.200



CONCLUSIONS

Table 1 indicates the influence of radial displacement on survival estimates. Referring to the case of 15-mil deflection, the maximum SCFS stress is 2.42 ksi and the associated stressed volume is 0.962 in^3 . Eq. 7 and the SPT diagram (Figure 10) can be used to estimate, at 99% P_s , that such a stress could be sustained for more than 20 years.

It should be recalled, however, that the data used to construct the SPT diagram was obtained under ambient laboratory conditions and it is assumed these represent the radome environment. More severe environments would lead to shorter life estimates. So-called inert strength could be measured at higher strain rates in a benign atmosphere, whereas slow strain rate results could be obtained in aqueous or other detrimental environments. Such data would most likely lead to significantly shorter life estimates. Note that the SCFS material used to generate the SPT diagram was machined from flat billets, using similar slip and generally identical processing techniques as in radome manufacture. However, it is a moot point whether this SCFS is indeed representative of radome materials. Preliminary tests on Type I radome fragments conducted at loading rates varying from 0.01 to 1.0 in./min suggested a potential range of slow crack exponent of $14 \leq n \leq 35$. Using the Weibull exponent of 10.3, which resulted from a best fit of 44 hydroburst tests on SCFS, and $n = 35.1$, the shortest life is estimated as 36 days for the 2.42 ksi stress maximum.

FREESE, *NEAL, and LENOE

Referring to Table 1, use of the various coefficients of variation is intended to represent potential uncertainties in the analytical modeling and associated stress distributions. For the largest radial deflection, the P_s estimates are observably affected. This emphasizes the necessity to accurately describe stress distributions. It is apparent that other proof test methods should be analyzed in detail and compared to design condition stresses to assess the adequacy of these screening techniques.

In summary, techniques have been discussed which permit estimates of probability of survival under fast fracture as well as sustained stress conditions. These analytical computations are quite sensitive to values of m and n . Therefore, it is imperative that actual radome materials be thoroughly characterized.

ACKNOWLEDGMENTS

The authors are indebted to the following individuals: P. Ormsby and J. Pemberton of MIRADCOM for supplying the slip-cast fused silica; R. Peters and G. Driscoll of AMMRC for conducting the experiments; D. Mason of AMMRC for assisting in the calculations, and to the staff of the Technical Reports Office for excellent preparation of the manuscript.

REFERENCES

1. WEIBULL, W. Proc. Ing. Vetenskapsakad Akad., 1939, p. 151.
2. FREUDENTHAL, A. M., in Fracture, An Advanced Treatise, v. II, Academic Press, New York, 1968, p. 591-619.
3. CHARLES, R. J. J. Appl. Phys., v. 29, no. 11, 1958, p. 1549-1560; also v. 29, no. 12, 1958, p. 1657-1667.
4. DAVIDGE, R. W., McLAREN, J. R., and TAPPIN, G. J. Matl. Sci., v. 8, December 1973, p. 1699-1705.
5. WIEDERHORN, S. M., in Fracture Mechanics of Ceramics, Plenum Press, New York, 1973, p. 613-646.
6. Ceramics for High Performance Applications, Part II, 1977, in press.
7. Production Specification for the Impregnated or Non-Impregnated Ceramic Radome in a Semi-Finished Form, MIS-20074B Code Ident. 18876, 26 February 1974.
8. WEIL, N. A., and DANIEL, I. M. J. Am. Ceram. Soc., v. 47, June 1964, p. 268-274.
9. BATDORF, S. B., in Proceedings of Intl. Symp. on Fracture Mechanics of Ceramics, Pennsylvania State University, July 27-29, 1977.
10. HOEL, P. G. *Introduction to Mathematical Statistics*. 4th ed., John Wiley and Sons, 1971.
11. FREESE, C. E. *An Efficient Substructuring Procedure for Axisymmetric Finite Element Analysis*. In preparation.
12. HAUGEN, E. B. *Probabilistic Approaches to Design*. John Wiley and Sons, 1968.